PCCP

Systematic study of ionic conduction in silver iodide/mesoporous alumina composites 3: Effects of binary silver halide doping

Journal:	*Physical Chemistry Chemical Physics*
Manuscript ID	CP-ART-12-2024-004865.R1
Article Type:	Paper
Date Submitted by the Author:	26-Feb-2025

Complete List of Authors:	Fukui, Yoko; NBC Meshtec Inc Yoshida, Yukihiro; Kyoto Daigaku, Division of Chemistry, Graduate School of Science Kitagawa, Hiroshi; Kyoto Daigaku, Division of Chemistry, Graduate School of Science Jikihara, Yohei; NBC Meshtec Inc

ARTICLE

Systematic study of ionic conduction in silver iodide/mesoporous alumina composites 3: Effects of binary silver halide doping†

Received 00th January 20xx,
Accepted 00th January 20xx

DOI: 10.1039/x0xx00000x

Yoko Fukui,*[a] Yukihiro Yoshida,*[b] Hiroshi Kitagawa[b] and Yohei Jikihara[a]

In our previous report (Y. Fukui *et al.*, *Phys. Chem. Chem. Phys.*, 2024, **26**, 13675), we reported the effect of AgBr-doping in AgI-loaded mesoporous alumina (MPA) composite on the phase stability and Ag^+-ion conductivity. This study revealed that the AgI-AgBr/MPA composites showed the highest room-temperature conductivity ($\sigma_{25°C}$) of 1.6×10^{-3} S cm^{-1} when AgBr content was 10 mol%, which is more than twice as high as that of the parent AgI/MPA composite (7.2×10^{-4} S cm^{-1}). In the present study, we investigated for the first time the effect of binary silver halide doping (i.e., AgBr/AgCl) in the AgI/MPA composite on Ag^+-ion conducting behaviour using variable-temperature powder X-ray diffraction, differential scanning calorimetry, and electrochemical impedance spectroscopy measurements. The AgI-AgBr-AgCl/MPA composites formed a *β*/*γ*-AgI-structured ternary solid solution (*β*/*γ*-AgI$_{ss}$) phase when the AgX (X = Br and Cl) content was 10 mol% (**Br5Cl5**), and underwent phase separation into *β*/*γ*-AgI$_{ss}$ and face-centred cubic structured ternary solid solution (AgBrCl$_{ss}$) when the AgX content was 20 mol% (**Br10Cl10**). Owing to the absence of phase separation, **Br5Cl5** showed a higher $\sigma_{25°C}$ value (1.1×10^{-3} S cm^{-1}) than that of **Br10Cl10** (9.0×10^{-4} S cm^{-1}), though both surpassed the value of the parent AgI/MPA. However, the conductivity of the AgI-AgBr-AgCl/MPA composites was lower than that of AgI-AgBr/MPA composites with the same doping levels. This result must reflect the importance of Ag^+···halide Coulomb interactions over Frenkel defects, which arise from the lattice distortion induced by the partial substitution of I^- ions with a smaller X^- (X = Br or Cl) ions. In addition, it could be described that this study marks the first successful synthesis of ternary silver halide nanoparticles with the aid of porous space.

Introduction

In recent years, solid electrolytes have significantly contributed to the advancement of high-performance electrical devices including batteries and sensors.[1–7] Unlike conventional liquid electrolytes, solid electrolytes offer several potential advantages, such as the elimination of leakage risks, excellent chemical stability, and high mechanical strength. These factors ensure the enhanced safety and longevity of batteries. In particular, Ag^+-ion solid electrolytes have garnered attention because of their high ionic conductivity and excellent chemical stability.[8–12] The soft acid nature of the Ag^+ ions facilitates the increased susceptibility to ionic polarisation, which promotes the ion migration in the anionic lattice.[13] Among the Ag^+-ion conductors, it is known that the high-temperature *α*-phase of silver iodide (AgI), which is composed of half-melted Ag^+ ions in the immobile I^- sublattice (> 147 °C), exhibits an exceptionally high ionic conductivity (ca. 1 S cm^{-1}).[14–18] Furthermore, an increase in the interstitial Ag^+-ion concentration in the low-temperature *β*/*γ*-phase can enhance the Ag^+-ion conductivity to reach a level required for the above-mentioned practical applications at room temperature. In this regard, it is known that the transference number of AgI at room temperature was estimated to be nearly unity.[19] To this end, there are several promising approaches as follows; (ⅰ) the construction of a heterogeneous interface between AgI and dielectric insulator (to form the space-charge layer),[20–53] (ⅱ) the reduction of particle size of AgI (to increase the surface energy),[54–58] and (ⅲ) the solid solution with homovalent ions of different ionic radii (to induce local distortion).[59–72] These approaches can facilitate the generation of Frenkel pairs comprising an interstitial Ag^+ ion and an Ag^+-ion vacant site, thereby leading to the increased Ag^+-ion conductivity.

Recently, our group implemented the optimisation of the pore size of insulating mesoporous alumina (MPA) to accommodate the AgI nanoparticles (i.e., (i) and (ii); hereafter AgI/MPA)[73] followed by the optimisation of the doping level of silver bromide (AgBr) with a smaller Br^- ion in AgX (X = I and Br)-loaded MPA composites (i.e., (iii); hereafter AgI-AgBr/MPA).[74] Thus it is apparent that the conducting pathway for Ag^+ ions is present at the interface between the surface of silver halide nanoparticles and the pore surface of MPA.

We have investigated the variable-temperature structural, calorimetric, and ion-conducting properties of AgX/MPA composites as follows;

(1) Pore size dependence in AgI/MPA (pore diameter: 2.4–15.9 nm for MPA): Ag^+-ion conductivity was the highest when MPA with a moderate pore size (7.1 nm) was used (7.2×10^{-4} S cm^{-1} at 25 °C).[73]

(2) AgI-loading ratio dependence in AgI/MPA (volumetric doping ratio: 1:9–8:2 for AgI/MPA): Ag^+-ion conductivity increased with increasing the filling ratio of AgI into the mesopores of MPA until the

[a] *NBC Meshtec Inc., 2-50-3 Toyoda, Hino, Tokyo 191-0053, Japan. E-mail: fukui.yoko@nisshin.com*
[b] *Division of Chemistry, Graduate School of Science, Kyoto University, Kitashirakawa-Oiwakecho, Sakyo-ku, Kyoto 606-8502, Japan. E-mail: yoshiday@ssc.kuchem.kyoto-u.ac.jp*

† Electronic Supplementary Information (ESI) available: Figs. S1–S5. See DOI: 10.1039/x0xx00000x

complete filling.[73]

(3) AgBr-doping ratio dependence in AgI-AgBr/MPA (AgBr content: 0–30 mol%): Ag^+-ion conductivity was the highest when the AgBr content was 10 mol% (1.6×10^{-3} S cm^{-1} at 25 °C).[74]

To the best of our knowledge, these studies represent the first simultaneous implementation of the three aforementioned approaches to achieve high Ag^+-ion conductivity in the *β*/*γ*-AgI phase.

In this study, a much smaller Cl^- ion (ionic radius: 1.81 Å vs. 1.96 Å for Br^- and 2.19 Å for I^- [75,76]) was introduced into the mesopores of MPA with the expectation of further introduction of Frenkel defects through lattice distortion in the AgI-AgBr/MPA composite. We measured variable-temperature powder X-ray diffraction (PXRD), differential scanning calorimetry (DSC), and AC impedance spectra of two types of ternary AgX (X = I, Br, and Cl)-loaded MPA composites; one with a homogeneous *β*/*γ*-AgI phase and another with phase separation into *β*/*γ*-AgI and face-centred cubic (fcc) phases, to extensively investigate the effect of the binary AgX (X = Br and Cl)-doping in the AgI/MPA composite on Ag^+-ion conducting behaviour.

Table 1 Composition ratios of AgX (X = I, Br, and Cl) in AgI-AgBr-AgCl/MPA composites and their notations

Notation	AgI (mol%)	AgBr (mol%)	AgCl (mol%)
Br5Cl5	90	5	5
Br10Cl10	80	10	10

Experimental section

Materials

In this study, we used commercially available MPA (Sigma-Aldrich Japan) with a pore diameter of 7.1 nm and a pore volume of 0.455 cm^3 g^{-1}, which were estimated based on the N_2 gas adsorption measurements (Fig. S1, ESI†). The MPA was dried at 500 °C for 6 h under N_2 atmosphere prior to use. AgI (99.0%, Kojima Chemicals Co., Ltd.), AgBr (97.0%, Wako Pure Chemical Industries, Ltd.), and AgCl (99.5%, Fujifilm Wako Pure Chemical Corporation, Ltd.) were dried at 200 °C for 6 h under N_2 atmosphere prior to use. Adequate amounts of dried silver halides and MPA to yield a volumetric filling ratio of approximately 90% were co-ground in an agate mortar under low humidity conditions in a N_2-filled glovebox (volumetric moisture content: < 0.35%). Each mixed powder was pressed at 500 MPa for 1 min to obtain a compressed pellet with a diameter of 2.5 mm, followed by heat treatment at 600 °C for 20 h to introduce AgX (melting point: 552, 432, and 455 °C for X = I, Br, and Cl, respectively) into the MPA pores.

Characterization

Room-temperature PXRD measurements were performed using a Bruker D8 ADVANCE instrument with Cu Kα radiation (λ = 1.5418 Å), whereas variable-temperature PXRD measurements were conducted using a Rigaku SmartLab instrument with Cu Kα radiation. The temperature was controlled using an Anton Paar DHS900 attachment with a rate of 5 °C min^{-1}. Rietveld refinements to evaluate the ratio of the phases with *α*-AgI, *β*/*γ*-AgI, and fcc AgX (X = Br and Cl)-like structures were performed with fixed atomic coordinates. Scanning electron microscope (SEM) observation and energy dispersive X-ray spectroscopy (EDS) analysis were performed using a JEOL JSM-IT500HR instrument at an accelerating voltage of 20 kV. The N_2 gas sorption isotherms were measured at 77 K using a MicrotracBEL BELSORP-mini Ⅱ volumetric adsorption system. Thermal properties were characterised by DSC thermograms using a NETZSCH DSC 3500 Sirius instrument equipped with N_2 cryostatic cooling. The composites, which were sealed in an aluminum pan, were heated from room temperature to 200 °C followed by cooling to 0 °C with a heating and cooling rate of 5 °C min^{-1}. Ionic conductivities of the compressed pellets were measured by the AC impedance technique with an applied voltage of 100 mV using a Solartron SI 1260 Impedance/Gain-phase Analyzer and 1260A Dielectric Interface in the frequency range of 1 MHz to 0.1 Hz. Both sides of the pellets were painted with gold paste (Tokuriki, 8560-1A) and measurements were performed in a temperature-controlled chamber (ESPEC ST-110). The impedance was determined from the first real axis touchdown point in the Nyquist plot.

Results and discussion

The AgX (X = Br and Cl)-loaded AgI/MPA composites (hereafter AgI-AgBr-AgCl/MPA) were prepared by co-grinding AgI/AgBr/AgCl in a molar ratio of 90:5:5 and 80:10:10 with MPA, followed by heat treatment at 600 °C (hereafter denoted as **Br5Cl5** and **Br10Cl10**, respectively; Table 1). All the peaks observed in the PXRD patterns of the mixtures before the heat treatment can be assigned to pristine *β*-AgI, *γ*-AgI, and trace amounts of fcc AgBr and AgCl phases (Fig. 1(a)). After the heat treatment, the fcc phases disappeared in the PXRD pattern of **Br5Cl5**, whereas an intense peak was observed at 30.3° in the pattern of **Br10Cl10** (Fig. 1(b)). Therefore, **Br5Cl5** is considered to form a homogeneous solid solution with *β*/*γ*-AgI-type structures, where AgBr and AgCl were dissolved into the AgI lattice (hereafter *β*/*γ*-AgI$_{ss}$). On the other hand, **Br10Cl10** underwent phase separation into *β*/*γ*-AgI$_{ss}$ and fcc AgX (X = Br and Cl)-structured solid solution (hereafter AgBrCl$_{ss}$) possibly due to the solid solubility limit of AgX in *β*/*γ*-AgI$_{ss}$, where the peak at 30.3° is assigned to the (200) reflection of the AgBrCl$_{ss}$ phase. The reflection was shifted toward a lower angle compared with that of the parent bulk AgBr (i.e., 30.3° for **Br10Cl10** vs. 30.9° for the parent

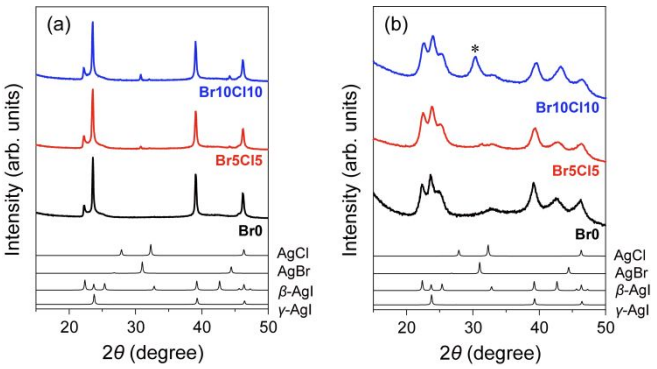

Fig. 1 PXRD patterns of AgI-AgBr-AgCl/MPA composites (a) before and (b) after the heat treatment at 600 °C for 20 h (red: **Br5Cl5**, blue: **Br10Cl10**), along with those of parent AgI/MPA composite (black: **Br0**). Black lines show the simulated patterns of AgCl, AgBr, *β*-AgI, and *γ*-AgI (from the top). An asterisk indicates the (200) reflection of the AgBrCl$_{ss}$ phase.

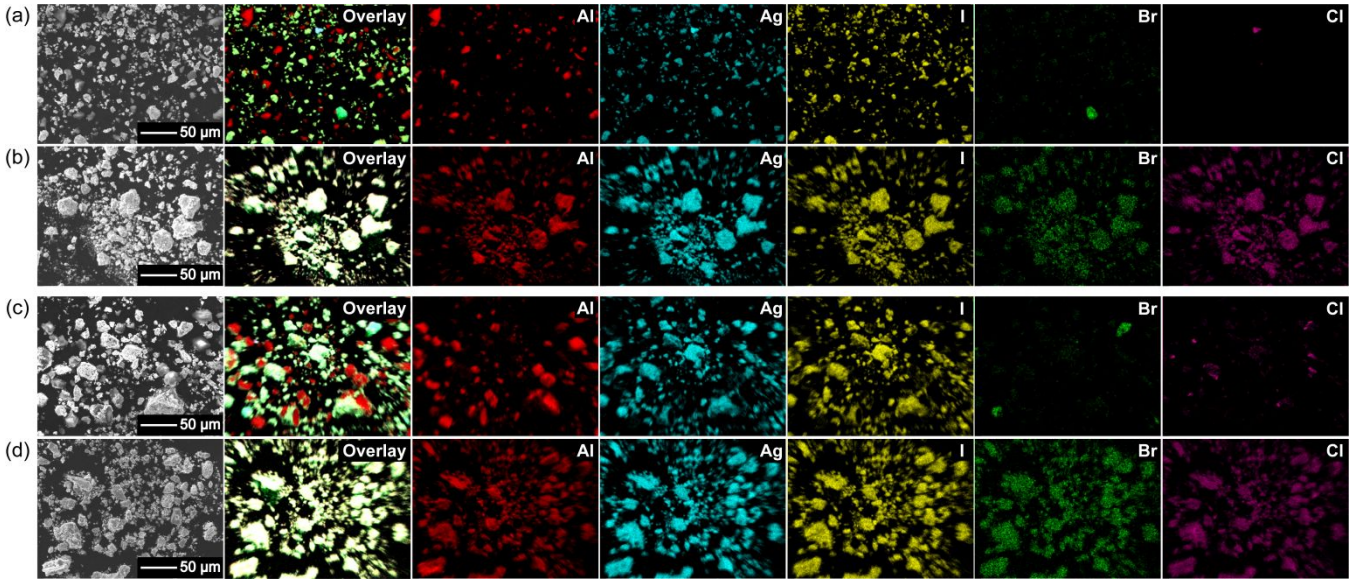

Fig. 2 SEM images and EDS mappings (Overlay, Al, Ag, I, Br, and Cl) of **Br5Cl5** (a) before and (b) after the heat treatment and **Br10Cl10** (c) before and (d) after the heat treatment.

bulk AgBr). Thus, the lattice constant estimated from the (200) peak is larger than that of the parent bulk AgBr (i.e., 5.90 Å for **Br10Cl10** vs. 5.78 Å for the parent bulk AgBr), clearly indicating that AgI is dissolved into the $AgBrCl_{ss}$ phase to form a ternary solid solution. The molar ratio of β/γ-AgI_{ss} and $AgBrCl_{ss}$ was estimated to be 65:35 under the assumption that the I/Br/Cl ratios at halogen sites in β/γ-AgI_{ss} and $AgBrCl_{ss}$ are equal to the nominal ratio. Upon heat treatment, the PXRD peaks of the composites became broadened, suggesting the reduced particle size of silver halides due to their introduction into the mesopores of MPA. We note that the crystallite sizes estimated from the PXRD patterns (7.6 nm for **Br5Cl5** and 7.1 nm for **Br10Cl10**; Fig. S2, ESI†) are comparable to the pore diameter of MPA (7.1 nm). To confirm the introduction of the silver halides into the MPA pores, EDS mappings of **Br5Cl5** and **Br10Cl10** were performed before and after the heat treatment. Whereas a distinct separation between Al and Ag/I/Br/Cl was observed in the mapping images taken before the heat treatment (Fig. 2(a) and (c)), the heat treatment led to a homogeneous elemental distribution for both composites (Fig. 2(b) and (d)). This result corroborates the successful introduction of silver halides into the mesopores of MPA, although the phase separation of β/γ-AgI_{ss} and $AgBrCl_{ss}$ in **Br10Cl10** evidenced by PXRD was not visible in the EDS mapping. This is indicative of randomly distributed β/γ-AgI_{ss} and $AgBrCl_{ss}$ phases in MPA at the micrometre scale. Furthermore, the

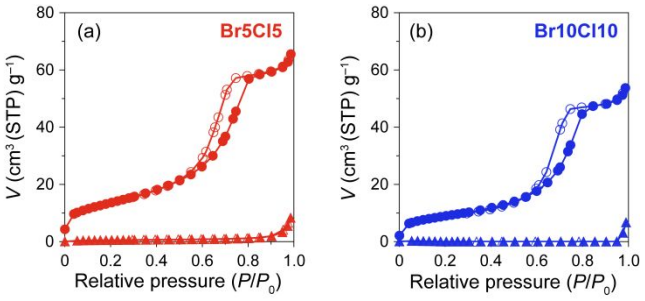

Fig. 3 N_2 gas adsorption (closed symbols) and desorption (open symbols) isotherms of (a) **Br5Cl5** and (b) **Br10Cl10** before (circles) and after (triangles) heat treatment.

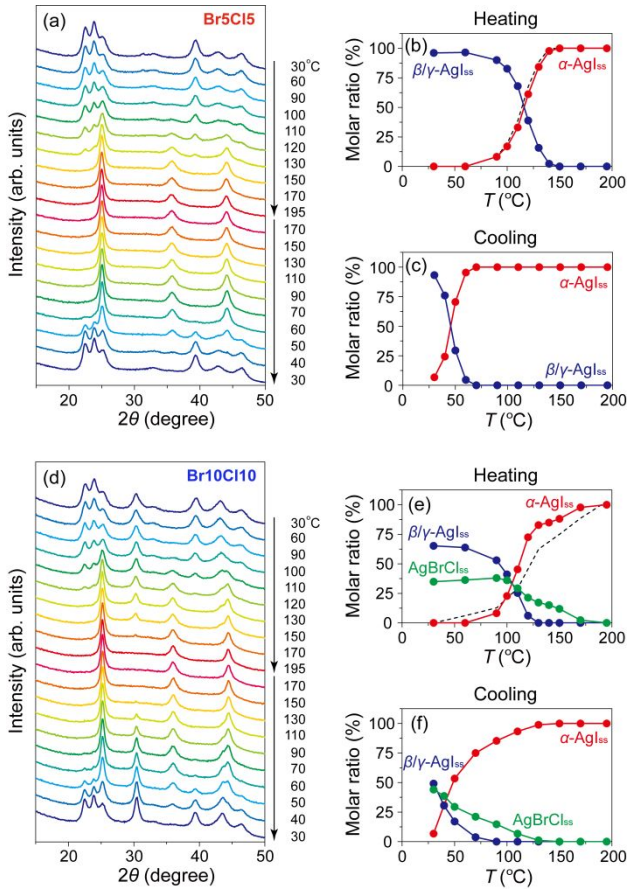

Fig. 4 (a) Variable-temperature PXRD patterns of (a) **Br5Cl5** and (d) **Br10Cl10** in the heating and cooling processes. Temperature dependences of the molar ratios of α- (red) and β/γ- (blue) AgI_{ss} phases of **Br5Cl5** in the (b) heating and (c) cooling processes and the molar ratios of α-AgI_{ss} (red), β/γ-AgI_{ss} (blue), and $AgBrCl_{ss}$ (green) phases of **Br10Cl10** in the (e) heating and (f) cooling processes. The black dotted lines in (b) and (e) indicate those of α-AgI_{ss} in **Br10** and **Br20**,[74] respectively. The ratios were determined by the Rietveld analysis.

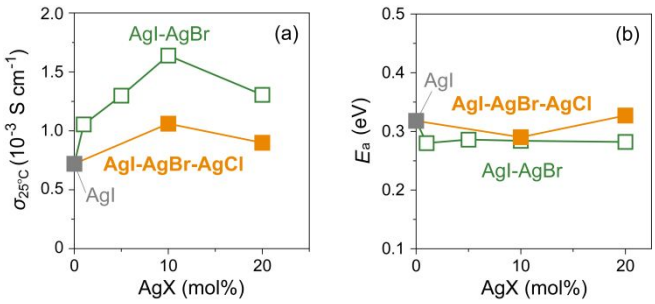

Fig. 5 (a) Room-temperature ionic conductivity ($\sigma_{25°C}$) and (b) activation energy (E_a) against AgX (X = Br and Cl)-doping ratio for AgI-AgBr-AgCl/MPA composites represented by orange closed squares. Green open squares represent the values of the AgI-AgBr/MPA composites doped with only AgBr,[74] whereas grey closed squares represent the values of parent AgI/MPA composite.[73]

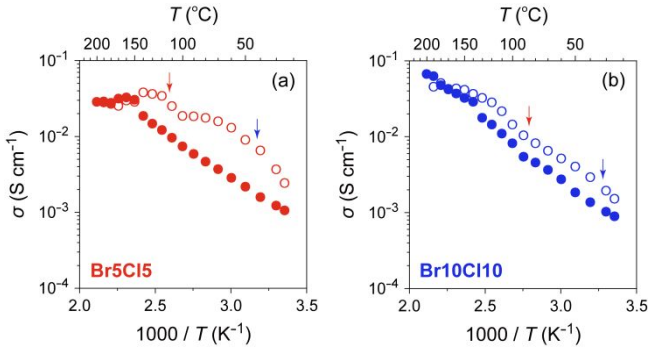

Fig. 6 Temperature dependence of ionic conductivity (σ) of (a) **Br5Cl5** and (b) **Br10Cl10** in heating (closed circles) and cooling (open circles) processes. The red and blue arrows indicate the onset temperatures of the transition on the high- and low-temperature sides, respectively, in the DSC cooling process (Fig. S3, ESI†).

introduction of silver halides into the mesopores of MPA was confirmed by N_2 gas sorption measurements; the mesopores manifested in a significant adsorption at $P/P_0 \sim 0.7$, which is characteristic of type IV in the IUPAC nomenclature, disappeared upon heat treatment (Fig. 3). This observation is consistent with our previous study that the pore volume gradually decreases with increasing the AgI-loading ratio.[73] A slight upturn in the high P/P_0 region is associated with the macropores from the inter-particulate voids of MPA. To the best of our knowledge, this is the first report that three types of silver halides, AgI, AgBr, and AgCl, have been simultaneously introduced into mesoporous materials to form the ternary solid solutions. In addition, it is plausible to say that we could synthesize the sub-ten nanometre-sized ternary silver halide nanoparticles for the first time in the mesopores of MPA.

Variable-temperature PXRD measurements of the solid-solution **Br5Cl5** and phase-separated **Br10Cl10** were performed to investigate the thermodynamic properties including phase transitions. Fig. 4(a) shows the PXRD patterns of **Br5Cl5** at various temperatures during the heating and cooling processes. The PXRD patterns showed the gradual disappearance of the β/γ-AgI_{ss} peaks above ca. 100 °C as the peaks of the α-AgI-structured solid-solution phase (hereafter denoted as α-AgI_{ss}) emerged concurrently. The PXRD patterns above ca. 150 °C exhibited only the α-AgI_{ss} peaks at $2\theta \sim 25$, 36, and 44°. The phase transition behaviour is more pronounced when the ratio of both phases determined by the Rietveld method is plotted as a function of temperature (Fig. 4(b) and 4(c)). In the subsequent cooling process, the α-AgI_{ss} phase remained stable down to ca. 60 °C, below which it transformed reversibly to the β/γ-AgI_{ss} phase. The observed thermal hysteresis occurs associated with a first-order transition, and the phase transition behaviour is fully consistent with the AgI-AgBr/MPA composite with the same doping level (hereafter denoted as **Br10**).[74] Fig. 4(d) displays the PXRD patterns of **Br10Cl10**, which underwent phase separation into β/γ-AgI_{ss} and $AgBrCl_{ss}$ at room temperature, at various temperatures. On heating, the peaks of β/γ-AgI_{ss} and $AgBrCl_{ss}$ began to disappear at approximately 100 °C with the concurrent appearance of the α-AgI_{ss} peaks, and eventually disappeared completely at 130 °C for β/γ-AgI_{ss} and 170 °C for $AgBrCl_{ss}$. The Rietveld analyses were performed under the assumption that the I/Br/Cl ratios in β/γ-AgI_{ss}, α-AgI_{ss}, and $AgBrCl_{ss}$ are equal to the nominal ratio. The molar ratio of β/γ-AgI_{ss} and $AgBrCl_{ss}$ in **Br10Cl10** was estimated to be 65:35 at 30 °C as mentioned above (Fig. 1(b)), which is strikingly different from 37:63 of β/γ-AgI_{ss} and $AgBr_{ss}$ in the AgI-AgBr/MPA composite with the same doping level (hereafter denoted as **Br20**).[74] Considering the previous observation that AgI is less soluble in the AgBr-AgCl solid solution than in AgBr,[77] the phase separation to form the $AgBrCl_{ss}$ phase must be suppressed in **Br10Cl10** including AgI as the dominant component. The α-AgI_{ss} phase of **Br10Cl10**, which began to appear at approximately 100 °C (Fig. 4(e)), is more prone to forming the homogeneous single phase at lower temperatures compared to **Br20**. Our previous study[74] revealed that the phase transition from β/γ- to α-phase occurs steadily at lower temperature in the AgI-AgBr/MPA composites with a homogeneous β/γ-AgI_{ss} phase (i.e., AgBr $\leq$ 10 mol%) than those with phase-separated β/γ-AgI_{ss} and $AgBr_{ss}$ (i.e., AgBr > 10 mol%), and therefore, the high β/γ-AgI_{ss}/$AgBrCl_{ss}$ ratio in **Br10Cl10** (65:35) is possibly responsible for the observed phase transition behaviour. On cooling, the α-AgI_{ss} phase in **Br10Cl10** remained stable until approximately 130 °C, below which it gradually and reversibly transformed into the β/γ-AgI_{ss} and $AgBrCl_{ss}$ phases (Fig. 4(f)). These gradual transitions are associated with the broad exothermic peak observed in the DSC profile (Fig. S3, ESI†).

The ionic conductivity (σ) of the AgI-AgBr-AgCl/MPA composites was measured using AC impedance spectroscopy. The room-temperature value ($\sigma_{25°C}$) of **Br5Cl5** and **Br10Cl10** were estimated to be 1.1×10^{-3} and 9.0×10^{-4} S cm^{-1}, respectively, which are more than three orders of magnitude higher than that of bulk AgI with β/γ-phase (ca. 1.5×10^{-7} S cm^{-1}).[54] Fig. 5(a) presents the AgX-doping ratio dependence of $\sigma_{25°C}$ in the AgI-AgBr-AgCl/MPA composites along with that in the AgI-AgBr/MPA composites[74] for comparison. The AgI-AgBr-AgCl/MPA composites exhibited a higher $\sigma_{25°C}$ than that of the parent AgI/MPA composite (i.e., **Br0**; 7.2×10^{-4} S cm^{-1}), because the Ag^+-ion migration was possibly promoted by the increased concentration of Frenkel pairs comprising an interstitial Ag^+ ion and an Ag^+-ion vacant site.[78,79] However, the $\sigma_{25°C}$ value of **Br10Cl10** is lower than that of **Br5Cl5**, as in the case of AgI-AgBr/MPA composites (i.e., **Br10** vs. **Br20**, where **Br10** represents AgI-AgBr/MPA composite doped with 10 mol% AgBr).[73] This must

be a consequence of the phase separation, namely the presence of $AgBrCl_{ss}$ phase in **Br10Cl10**, which suppresses the Ag^+-ion migration.[39,61,67] The AgI-AgBr-AgCl/MPA composites exhibited a lower $\sigma_{25°C}$ value than that of AgI-AgBr/MPA composites with the same doping level, even though a further introduction of the Frenkel defects is expected due to the lattice distortion induced by the partial substitution of Br^- with Cl^- in the lattice. This change in conducting behaviour can be attributed to the increased Coulomb interactions between mobile Ag^+ ions and immobile X^- ions due to the higher electronegativity of Cl^- ions than that of Br^- ions.[80,81] In other words, the possible stimulation of Ag^+-ion migration by the increased concentration of Frenkel defects was suppressed by the Coulomb interactions with Cl^- ions with a lower covalent-bonding nature.

Fig. 6 shows the temperature dependence of σ for **Br5Cl5** and **Br10Cl10** in the temperature range of 25–200 °C. Upon heating, **Br5Cl5** exhibited an Arrhenius-type ionic conduction up to approximately 140 °C (Fig. 6(a)), whereas **Br10Cl10** showed a nearly continuous increase in σ with increasing temperature up to the highest measured temperature (i.e., 200 °C) without any significant change in slope (Fig. 6(b)). This behaviour in **Br10Cl10** is reminiscent of that observed in phase-separated **Br20**.[74] It is most likely that the suppression of the discontinuous σ change in **Br10Cl10**, which is associated with the phase transition from the low-conducting β/γ-phase to the superionic α-AgI phase (as observed for bulk AgI), is caused by the phase separation as confirmed by the PXRD studies. The activation energy (E_a) values for the AgI-AgBr-AgCl/MPA composites were estimated by fitting the experimental data up to 130 °C to the Arrhenius equation, $\sigma T = A \exp(-E_a/k_B T)$, where A is the pre-exponential factor and k_B is the Boltzmann constant. The E_a value of silver halides is generally expressed as $E_a = H_f/2 + h_m$, where H_f is the formation enthalpy of Frenkel defects and h_m is the migration energy of Frenkel defects.[82] As shown in Fig. 5(b), the E_a values of the AgI-AgBr-AgCl/MPA composites remained relatively unchanged with varying AgX (X = Br and Cl) contents, as in the case of the AgI-AgBr/MPA composites.[74] In addition, the E_a value of **Br5Cl5** (0.29 eV) is comparable to that of **Br10** (0.28 eV) despite the fact that **Br5Cl5** includes smaller Cl^- ions in the β/γ-AgI_{ss} phase. Furthermore, the β/γ-AgI_{ss} lattice of **Br5Cl5** is more distorted than that of **Br10**, which must lead to a reduced H_f value of **Br5Cl5**. Thus the comparable E_a values are apparently caused by the larger h_m value of **Br5Cl5** than that of **Br10** primarily driven by the increased Coulomb $Ag^+\cdots X^-$ interactions as mentioned above; namely, the larger h_m value compensates for the smaller H_f value, leading to comparable E_a values. As shown in Fig. S4 (ESI†), the ionic conductivity at 200 °C ($\sigma_{200°C}$) of **Br10Cl10** (6.7×10^{-2} S cm^{-1}) is higher than those of **Br0** (3.1×10^{-2} S cm^{-1}) and **Br5Cl5** (2.9×10^{-2} S cm^{-1}), which is possibly associated with the large crystallite size of the superionic α-AgI_{ss} phase (**Br10Cl10** (8.5 nm) ~ **Br0** (8.5 nm) > for **Br5Cl5** (6.6 nm) at 195 °C) as well as the high thermodynamic stability of the superionic α-AgI_{ss} phase (**Br10Cl10** ~ **Br5Cl5** > **Br0**) as confirmed by the variable-temperature PXRD measurements.[73,74]

During the cooling process, the ion-conducting behaviour of **Br5Cl5** is significantly different from that observed during the heating process, whereas that of **Br10Cl10** does not differ significantly from that in the heating process. In **Br5Cl5**, the temperatures at which the σ value significantly drops correspond approximately to the onset temperatures of the exothermic DSC peaks observed during the cooling process (Fig. S3, ESI†). In our previous study,[73] the DSC peaks observed in AgI/MPA composites were ascribed to the phase transition from α- to β/γ-phases of AgI particles occupying the core of the pores for the high-temperature peak and near the surface of the pores for the low-temperature peak (Fig. S5, ESI†). Thus, the non-Arrhenius ion-conducting behaviour observed for **Br5Cl5** is thought of as a manifestation of the distinct structural transition from α- to β/γ-AgI_{ss} phases. In contrast, the Arrhenius-like temperature dependence of σ in **Br10Cl10** is associated with the gradual formation of β/γ-AgI_{ss} and $AgBrCl_{ss}$ phases indicated by the PXRD (Fig. 4) and DSC (Fig. S3, ESI†) data.

Conclusions

In this study, for the first time, we succeeded in simultaneously introducing three types of silver halides into the mesopores of MPA to form a homogeneous solid solution. **Br5Cl5** with the halide ratio of I/Br/Cl = 90:5:5 formed a solid solution phase with β/γ-AgI-type structures, whereas **Br10Cl10** with the halide ratio of I/Br/Cl = 80:10:10 underwent phase separation into β/γ-AgI and fcc phases at room temperature. This work also demonstrated the first synthesis of the sub-ten nanometre-sized ternary silver halide nanoparticles with the aid of porous space. The purpose of this work was to further increase the ionic conductivity of AgI/AgBr-loaded MPA composites by doping AgCl with a smaller Cl^- to increase the concentration of Frenkel defects induced by lattice distortion. However, contrary to our expectations, the AgCl-doping apparently reduced Ag^+-ion migration compared to the AgI-AgBr/MPA composites doped only with AgBr. The decreased conductivity is attributed to the increased $Ag^+\cdots X^-$ Coulomb interaction when X is a highly electronegative Cl, which interferes with the Ag^+-ion migration. Our findings indicate that the Ag^+-ion conducting behaviour in the present hybrid system is primarily governed by a delicate equilibrium between the concentration of Frenkel defects through the distortion of the immobile sublattice and the softness of the sublattice, i.e., Coulomb interactions with mobile Ag^+ ions.

Conflicts of interest

There are no conflicts to declare.

Acknowledgements

This work was supported by the ACCEL program (JPMJAC1501) of the Japan Science and Technology Agency (JST) and JSPS KAKENHI Grant Numbers JP20H02708 and JP20H05623. Variable-temperature PXRD measurements were conducted at the University of Tokyo, supported by "Advanced Research Infrastructure for Materials and Nanotechnology in Japan (ARIM)" of the Ministry of Education, Culture, Sports, Science and Technology (MEXT), Grant Number JPMXP1223UT0224.

Notes and references

1 P. Knauth and J. Schoonman, *Nanostructured Materials: Selected Synthesis Methods, Properties and Applications*, Kluwer Academic Publishers, Dordrecht, 2002.
2 T. Minami, M. Tatsumisago, M. Wakihara, C. Iwakura, S. Kohjiya and I. Tanaka, *Solid State Ionics for Batteries*, Springer, Tokyo, 2005.
3 J. Schoonman, *Solid State Ionics*, 2000, **135**, 5–19.
4 P. Knauth and H. L. Tuller, *J. Am. Ceram. Soc.*, 2002, **85**, 1654–1680.
5 K. Funke, *Sci. Technol. Adv. Mater.*, 2013, **14**, 043502.
6 Z. Zou, Y. Li, Z. Lu, D. Wang, Y. Cui, B. Guo, Y. Li, X. Liang, J. Feng, H. Li, C. W. Nan, M. Armand, L. Chen, K. Xu and S. Shi, *Chem. Rev.*, 2020, **120**, 4169–4221.
7 F. Wu, L. Liu, S. Wang, J. Xu, P. Lu, W. Yan, J. Peng, D. Wu and H. Li, *Prog. Mater. Sci.*, 2022, **126**, 100921.
8 B. Reuter and K. Hardel, *Angew. Chem.*, 1960, **72**, 138–139.
9 J. N. Bradley and P. D. Greene, *Trans. Faraday Soc.*, 1966, **62**, 2069–2075.
10 J. N. Bradley and P. D. Greene, *Trans. Faraday Soc.*, 1967, **63**, 424–430.
11 D. O. Raleigh, *J. Appl. Phys.*, 1970, **41**, 1876–1877.
12 S. Geller and B. B. Owens, *J. Phys. Chem. Solids*, 1972, **33**, 1241–1250.
13 R. G. Pearson, *J. Am. Chem. Soc.* 1963, **85**, 3533–3539.
14 C. Tubandt and E. Lorenz, *Z. Phys. Chem.*, 1914, **87U**, 513–542.
15 G. Cochrane and N. H. Fletcher, *J. Phys. Chem. Solids*, 1971, **32**, 2557–2567.
16 T. Takahashi, *J. Appl. Electrochem.*, 1973, **3**, 79–90.
17 K. Funke, *Prog. Solid State Chem.*, 1976, **11**, 345–402.
18 S. Hull, *Rep. Prog. Phys.*, 2004, **67**, 1233–1314.
19 B. V. R. Chowdari, S. Chandra, S. Singh and P. C. Srivastava, *Solid State Ionics; Materials and Applications: Proceedings of the 3rd Asian Conference*, 1992.
20 K. Shahi and J. B. Wagner Jr., *Solid State Ionics*, 1981, **3–4**, 295–299.
21 K. Shahi and J. B. Wagner Jr., *J. Electrochem. Soc.*, 1981, **128**, 6–13.
22 P. Chowdhary, V. B. Tare and J. B. Wagner Jr., *J. Electrochem. Soc.*, 1985, **132**, 123–124.
23 Z. Zhao, C. Wang, S. Dai and L. Chen, *Solid State Ionics*, 1983, **9–10**, 1175–1178.
24 S. Furusawa, S. Miyaoka and Y. Ishibashi, *J. Phys. Soc. Jpn.*, 1991, **60**, 1666–1671.
25 M. C. R. Shastry and K. J. Rao, *Solid State Ionics*, 1992, **51**, 311–316.
26 R. C. Agrawal and R. K. Gupta, *J. Mater. Sci.*, 1999, **34**, 1131–1162.
27 N. F. Uvarov, P. Vaněk, M. Savinov, V. Železný, V. Studnička and J. Petzelt, *Solid State Ionics*, 2000, **127**, 253–267.
28 J. Lee, S. Adams and J. Maier, *J. Electrochem. Soc.*, 2000, **147**, 2407–2418.
29 S. Mochizuki and F. Fujishiro, *J. Phys.: Condens. Matter*, 2003, **15**, 5057–5072.
30 F. Fujishiro and S. Mochizuki, *Physica B*, 2003, **340–342**, 216–220.
31 F. Fujishiro and S. Mochizuki, *Solid State Ionics*, 2009, **180**, 497–500.
32 B. J. Brownlee, L. Tsui, K. Vempati, J. B. Plumley, B. D. Iverson, T. L. Peng and F. H. Garzon, *J. Appl. Phys.*, 2020, **128**, 035103.
33 D. P. Lara, H. Correa and D. Suescún-Díaz, *Ionics*, 2022, **28**, 2911–2917.
34 M. Nagai and T. Nishino, *J. Electrochem. Soc.*, 1991, **138**, L49–L51.
35 M. Nagai and T. Nishino, *Solid State Ionics*, 1992, **53–56**, 63–67.
36 M. Nagai and T. Nishino, *J. Am. Ceram. Soc.*, 1993, **76**, 1057–1060.
37 M. Nagai and T. Nishino, *Solid State Ionics*, 1999, **117**, 317–321.
38 K. Tadagana, K. Imai, M. Tatsumisago and T. Minami, *J. Electrochem. Soc.*, 2000, **147**, 4061–4064.
39 H. Yamada, A. J. Bhattacharyya and J. Maier, *Adv. Funct. Mater.*, 2006, **16**, 525–530.
40 H. Yamada, I. Saruwatari, N. Kuwata and J. Kawamura, *J. Phys. Chem. C*, 2014, **118**, 23845–23852.
41 C. Liang, K. Terabe, T. Hasegawa and M. Aono, *J. Appl. Phys.*, 2007, **102**, 124308.
42 C. Liang, K. Terabe, T. Tsuruoka, M. Osada, T. Hasegawa and M. Aono, *Adv. Funct. Mater.*, 2007, **17**, 1466–1472.
43 H. Zhang, T. Tsuchiya, C. Liang and K. Terabe, *Nano Lett.*, 2015, **15**, 5161–5167.
44 L. Liu, S. Lee, J. Li, M. Alexe, G. Rao, W. Zhou, J. Lee, W. Lee and U. Gösele, *Nanotechnology*, 2008, **19**, 495706.
45 W. Lee, H. Yoo and J. Lee, *Chem. Commun.*, 2001, 2530–2531.
46 K. Tadagana, K. Imai, M. Tatsumisago and T. Minami, *J. Electrochem. Soc.*, 2002, **149**, A773–A777.
47 S. Albert, N. Frolet, P. Yot, A. Pradel and M. Ribes, *Solid State Ionics*, 2006, **177**, 3009–3013.
48 S. V. Baryshnikov, C. Tien, E. V. Charnaya, M. K. Lee, D. Michel, W. Böhlmann and N. P. Andriyanova, *Phys. Solid State*, 2008, **50**, 1342–1346.
49 S. V. Baryshnikov, C. Tien, E. V. Charnaya, M. K. Lee, D. Michel, W. Böhlmann and N. P. Andriyanova, *J. Phys.: Condens. Matter*, 2008, **20**, 025214.
50 A. Pradel, P. Yot, S. Albert, N. Frolet and M. Ribes, in *Nanostructured Materials for Advanced Technological Applications*, ed. J. P. Reithmaier, P. Petkov, W. Kulisch and C. Popov, Springer, Dordrecht, 2009, pp. 233–243.
51 P. G. Yot, S. Albert, N. Frolet, M. Ribes and A. Pradel, *J. Phys. Chem. C*, 2010, **114**, 18318–18322.
52 A. V. Il'inskii, R. A. Aliev, D. A. Kurdyukov, N. V. Sharenkova, E. B. Shadrin and V. G. Golubev, *Phys. Status Solidi A*, 2006, **203**, 2073–2077.
53 M. Reháková, M. Casciola, I. G. K. Andersen and Z. Bastl, *J. Incl. Phenom. Mol. Recognit. Chem.*, 1996, **25**, 303–312.
54 R. Makiura, T. Yonemura, T. Yamada, M. Yamauchi, R. Ikeda, H. Kitagawa, K. Kato and M. Takata, *Nat. Mater.*, 2009, **8**, 476–480.
55 S. Yamasaki, T. Yamada, H. Kobayashi and H. Kitagawa, *Chem. Asian J.*, 2013, **8**, 73–75.
56 T. Yamamoto, M. Maesato, N. Hirao, SI. Kawaguchi, S. Kawaguchi, Y. Ohishi, Y. Kubota, H. Kobayashi and H. Kitagawa, *J. Am. Chem. Soc.*, 2017, **139**, 1392–1395.
57 T. Yamamoto, H. Kobayashi, L. S. R. Kumara, O. Sakata, K. Nitta, T. Uruga and H. Kitagawa, *Nano Lett.*, 2017, **17**, 5273–5276.
58 T. Ida and K. Kimura, *Solid State Ionics*, 1998, **107**, 313–318.
59 K. Shahi and J. B. Wagner Jr., *Appl. Phys. Lett.*, 1980, **37**, 757–759.
60 K. Shahi and J. B. Wagner Jr., *Phys. Rev. B*, 1981, **23**, 6417–6421.
61 K. Shahi and J. B. Wagner Jr., *J. Phys. Chem. Solids*, 1982, **43**, 713–722.
62 K. Shahi and J. B. Wagner Jr., *Solid State Ionics*, 1984, **12**, 511–516.
63 L. S. Cain and L. M. Slifkin, *J. Phys. Chem. Solids*, 1980, **41**, 173–178.
64 S. Ihara, Y. Warita and K. Suzuki, *Phys. Status Solidi A*, 1984, **86**, 729–734.
65 M. Palanisamy, K. Thangaraj, R. Gobinathan and P. Ramasamy, *J. Mater. Sci.*, 1987, **22**, 670–674.
66 A. Yoshiasa, F. Kanamaru, S. Emura and K. Koto, *Solid State Ionics*, 1988, **27**, 267–274.

67 U. Lauer and J. Maier, *Solid State Ionics*, 1992, **51**, 209–213.
68 R. K. Gupta and R. C. Agrawal, *Solid State Ionics*, 1994, **72**, 314–317.
69 R. C. Agrawal, R. Kumar, R. K. Gupta and M. Saleem, *J. Non-Cryst. Solids*, 1995, **181**, 110–115.
70 M. Kusakabe, M. Arai, Y. Ito and S. Tamaki, *Solid State Ionics*, 1999, **121**, 295–299.
71 J. F. Jurado, J. A. Trujillo, B. -E. Mellander and R. A. Vargas, *Solid State Ionics*, 2003, **156**, 103–112.
72 A. Yuzhakova, D. Salimgareev, A. Turabi, A. Korsakov and L. Zhukova, *Opt. Laser Technol.*, 2021, **139**, 106995.
73 Y. Fukui, Y. Yoshida, H. Kitagawa and Y. Jikihara, *Phys. Chem. Chem. Phys.*, 2023, **25**, 25594–25602.
74 Y. Fukui, Y. Yoshida, H. Kitagawa and Y. Jikihara, *Phys. Chem. Chem. Phys.*, 2024, **26**, 13675–13682.
75 R. D. Shannon and C. T. Prewitt, *Acta Crystallogr. B*, 1969, **25**, 925–946.
76 R. D. Shannon, *Acta Crystallogr. A*, 1976, **32**, 751–767.
77 L. V. Zhukova, D. V. Shatunova, D. D. Salimgareev, A. E. Lvov, A. A. Yuzhakova, A. S. Korsakov and P. V. Pestereva, *J. Cryst. Growth*, 2024, **627**, 127528.
78 J. Maier, *Angew. Chem. Int. Ed. Engl.*, 1993, **32**, 313–335.
79 J. Maier, *Prog. Solid State Chem.*, 1995, **23**, 171–263.
80 T. L. Cottrell, *The Strengths of Chemical Bonds*, Academic Press Inc., New York, 1954.
81 T. L. Allen, *J. Chem. Phys.*, 1957, **26**, 1644–1647.
82 P. Müller, *Phys. Status Solidi*, 1965, **12**, 775–794.

Data Availability Statement

The original contributions presented in the study are included in the article/supporting information, further inquiries can be directed to the corresponding authors, YF (fukui.yoko@nisshin.com) and YY (yoshiday@ssc.kuchem.kyoto-u.ac.jp).

Supporting Information

The Supporting Information is available free of charge on the RSC Publications website;
N_2 gas sorption isotherms, DSC profiles, and doping ratio dependences of crystallite size, Ag^+-ion conductivity at 200 °C, and transition temperatures.